Available online at www.sciencedirect.com
ScienceDirect
Journal of Volcanology and Geothermal Research 169 (2008) 48–60
Journal of volcanology and geothermal research
www.elsevier.com/locate/jvolgeores

Transition between fragmentation and permeable outgassing of low viscosity magmas

Atsuko Namiki [a,b,*], Michael Manga [a]

[a] Department of Earth and Planetary Science, University of California, Berkeley, 307, McCone Hall, Berkeley, CA94720-4767, USA
[b] AIST, Institute of Geology and Geoinformation, Higashi 1-1-1 no. 7, Tsukuba, 305-8567 Japan

Received 16 February 2007; accepted 31 July 2007
Available online 29 August 2007

Abstract

Explosive volcanic eruption requires that magma fragments into discrete parcels. Silicic magma can fragment through brittle failure or other processes that depend on the viscoelasticity of the melt. Owing to the low viscosity of basaltic magmas, however, the fragmentation mechanism must be different and will be governed by fluid mechanics alone. We perform a series of decompression experiments on bubbly Newtonian fluids with viscosities and surface tensions similar to those of basaltic magmas. For sufficiently rapid expansion, the bubbly fluid expands continuously, eventually tearing into several pieces. We find that the fragmentation threshold is governed by a critical Reynolds number of ~1, indicating that it is the inertia of the expanding fluid that drives the continued expansion and ultimate breakup into discrete parcels. Experiments in which the fluid does not fragment allow us to determine the gas permeability of the bubbly fluid as the bubbles expand. Permeability remains small until the volume fraction of bubbles exceeds about 70%. We scale the results of the laboratory experiments to basaltic eruptions and find that the predicted fragmentation threshold is consistent with the exit velocities that characterize effusive and explosive eruptions. Our experimental results suggest that the mechanism for fragmentation of low viscosity basaltic magma is fundamentally different from that of high-viscosity silicic magma, and that magma with low viscosities can fragment easily.

Keywords: bubbly fluid; fragmentation; decompression; permeability; outgassing; basaltic magma; fire fountain

1. Introduction

The transition between explosive and effusive eruption is controlled by the ability of magma to break into discrete pieces (fragmentation) and the rate at which gases escape from the rising magma (outgassing). Fragmentation transforms the magma from one with a continuous melt phase and high viscosity to one with a continuous gas phase and much lower viscosity. Outgassing suppresses explosive eruption because it removes the gases that drive the eruption.

In silicic magmas there are two commonly invoked mechanisms and adopted criteria for fragmentation. One criterion that applies to viscoelastic glasses is that the strain rate exceeds $\sim 10^{-2} G/\eta_s$, where η_s is the melt shear viscosity at low strain rates, G is the shear modulus, and η_s/G is the structural relaxation time of the melt (Webb and Dingwell, 1990; Goto, 1999; Papale, 1999; Gonnermann and Manga, 2003; Tuffen et al.,

* Corresponding author. Now at Department of Earth Sciences, Kanazawa University, Kakuma, Kanazawa, Ishikawa 920-1192, Japan. Tel.: +81 76 264 6539; fax: +81 76 264 6545.
E-mail address: a-namiki@earth.s.kanazawa-u.ac.jp (A. Namiki).

0377-0273/$ - see front matter © 2007 Elsevier B.V. All rights reserved.
doi:10.1016/j.jvolgeores.2007.07.020

2003). A second fragmentation mechanism requires that the stresses in the films surrounding bubbles exceed the failure strength of the melt (e.g., McBirney and Murase, 1970; Zhang, 1999). This mechanism requires that the melt viscosity is high enough to inhibit bubble expansion so that large over-pressure develops inside the bubbles (Toramaru, 1995; Proussevitch and Sahagian, 1996; Navon et al., 1998; Lensky et al., 2004; Koyaguchi and Mitani, 2005).

Basaltic magmas can erupt both effusively and explosively. Explosivity of basaltic eruptions ranges from "weakly" explosive (Strombolian and sustained fountaining) to Plinian. Owing to the low viscosity of (low crystallinity) basaltic magmas, however, neither of the two fragmentation mechanisms that may apply in silicic magmas can occur during basaltic eruptions. First, the strain rate will never come close to the inverse relaxation time, except under exceptional conditions in which the magma has high viscosity because of low temperature produced by rapid cooling or high crystallinity (Giordano and Dingwell, 2003). Second, for typical decompression rates during explosive eruptions the viscosity required to retard bubble expansion is $>10^6$ Pa s (Thomas et al., 1994; Barclay et al., 1995; Gardner et al., 2000), and hence is much greater than the viscosity of basaltic melts. If magmas have high enough crystallinity that they develop an interconnected network of crystals (e.g., Saar et al., 2001), the finite strength of the magma may impede bubble growth and promote fragmentation in basaltic magmas (e.g., Houghton et al., 2004; Sable et al., 2006).

To quantify the outgassing process, the permeability of natural (Eichelberger et al., 1986; Klug and Cashman, 1996; Saar and Manga, 1999; Rust and Cashman, 2004; Muller et al., 2005), and laboratory (Takeuchi et al., 2005) magmas has been measured. Finite permeability requires an interconnected network of bubbles. Prior to eruption, the magma contains isolated, spherical bubbles and hence zero permeability. The development of permeability will be governed by the deformation of the magma and the expansion of bubbles which permit the rupture of the films of fluid separating individual bubbles. Outgassing plays a critical role in the evolution and characteristics of explosive basaltic eruptions (e.g., Houghton et al., 2004) and determining whether basaltic eruptions are explosive or effusive (e.g., Roggensack et al., 1997).

In the present paper we conduct a series of decompression experiments using bubbly fluids with viscosities and surface tensions similar to those for basaltic magma. We first determine the conditions under which the bubbly fluid fragments. Next we identify when the bubbly fluid becomes permeable and calculate its permeability. The experiments allow us to propose a fragmentation criterion for basaltic magma and a criterion for an expanding bubbly fluid to become permeable. In particular we show that if the inertia of the magma generated by bubble expansion is large enough, the magma can continue to expand and deform to the point that it fragments into discrete parcels. Finally, we show that these criteria are consistent with the conditions that characterize both explosive and effusive eruptions.

2. Experimental procedure

We conduct decompression experiments in the shock tube apparatus illustrated in Fig. 1. This is a widely used method to simulate the rapid decompression of analogue magmatic materials (e.g., Mader et al., 1997). The high-viscosity bubbly fluid is contained in the high-pressure shock tube and is separated from a large low-pressure tank by diaphragms. The diaphragms are made of either commercial aluminum foil or 5–20 μm thick polyester films. When the diaphragms break, a rarefaction wave propagates into the tube and the bubbly fluid is decompressed. The shock tube has an inner diameter of 0.05 m and a length of 0.25 m. The volume of the low-pressure tank is 0.18 m^3. The initial pressure in the shock tube P_h is variable between 7×10^4 and 3×10^5 Pa, and pressure inside the low-pressure tank P_l is approximately 2×10^4 Pa. The inside high-pressure tube is pressurized by CO_2 gas. The pressure during the decompression is

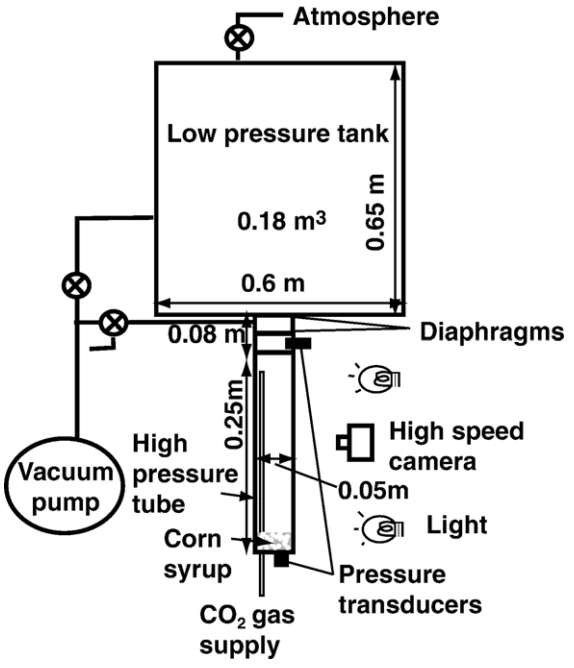

Fig. 1. Illustration of the experimental apparatus.

measured by pressure transducers located at the top and the bottom of the high-pressure tube and is recorded by an oscilloscope.

For our magma analogue, we use corn syrup solutions. By varying the water content of the corn syrup, we change its viscosity from 1 Pa s to 3×10^3 Pa s, and thus cover the typical viscosity range of basaltic melts (e.g., Spera, 2000). The shear viscosity of the corn syrup η_s is measured with a ThermoHaake Rheoscope cone-and-plate rheometer as a function of temperature and shear rate. For the range of shear rates in our measurements, the corn syrup behaves as a Newtonian fluid, and its viscosity is independent of shear rate. The lights used to illuminate the high-pressure tube during the experiment can heat the corn syrup and hence change its viscosity. Owing to the strong temperature-dependence of the viscosity of corn syrup, we monitored the temperature of the fluid in the shock tube and room temperature with thermocouples. The largest uncertainty in viscosity of our fluid is the uncertainty in temperature: we assume that the viscosity is in between the viscosity at the temperature in the high-pressure tube and room temperature and use this range of viscosities to define the uncertainty in viscosity.

Bubbles are created through a chemical reaction between baking soda and citric acid which generates carbon dioxide. The required time for the chemical reaction to generate bubbles depends on the fluid viscosity. Fig. 2 shows an example of bubbles generated by this reaction. This image is taken through a microscope and shows bubbles within the high-pressure tube immediately before the decompression. The bubbles are distributed homogeneously in the syrup, and exhibit a range of diameters with a mean close to 100 μm. The water content of the corn syrup, measured with a refractometer, was almost the same before and after the experiment, and we thus infer that the baking soda and citric acid do not affect the viscosity of corn syrup significantly. No surfactant is added to the corn syrup.

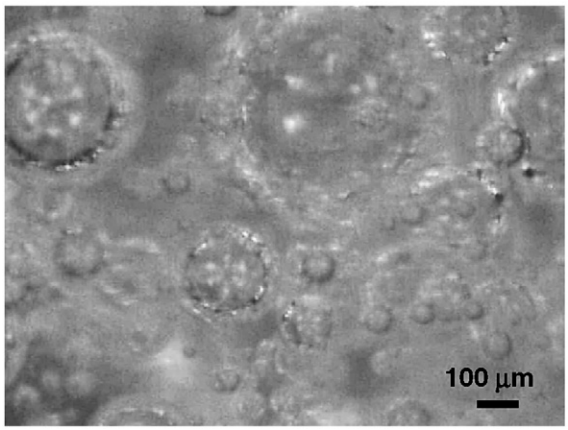

Fig. 2. Picture of bubbles within the fluid in the high-pressure tube that are generated by the chemical reaction of baking soda and citric acid. Picture is taken just before the decompression and is taken with a microscope.

Table 1
Experimental conditions and results. Viscosity is the mean value based on the temperature at the inside and outside of the high-pressure tube. In the column labeled "type" crosses and circles indicate that fragmentation is and is not observed, respectively

ϕ_i	Viscosity (Pa s)	P_h (10^5 Pa)	P_l (10^5 Pa)	Type
0.57	2.7×10^3	1.0	0.2	○
0.54	1.9×10^3	1.0	0.2	○
0.55	2.7×10^3	1.7	0.2	○
0.41	2.9×10^3	2.8	0.2	○
0.81	2.9×10^3	1.0	0.2	○
0.76	2.6×10^3	1.7	0.2	○
0.57	1.5×10^0	1.0	0.2	×
0.10	2.1×10^3	1.0	0.2	○
0.59	6.0×10^2	1.0	0.2	○
0.55	6.1×10^1	1.0	0.2	×
0.48	4.9×10^2	2.9	0.2	○
0.52	2.0×10^2	1.0	0.2	○
0.53	1.9×10^2	2.8	0.2	×
0.65	5.1×10^2	2.7	0.2	○
0.58	4.2×10^2	3.0	0.2	○
0.55	4.9×10^1	0.7	0.2	○
0.21	1.6×10^2	1.0	0.2	○
0.36	1.9×10^2	1.0	0.2	○
0.37	2.8×10^3	1.0	0.2	○
0.26	5.7×10^1	1.0	0.2	○
0.32	2.9×10^3	1.0	0.2	○
0.46	5.2×10^1	1.0	0.2	×

The experimental procedure is as follows. First, we stir the mixture of corn syrup, baking soda, and citric acid in a beaker, then pour it into the high-pressure tube. During this procedure, small amounts of air bubbles could be entrained in the corn syrup, however their volume is negligible compared to that of the carbon dioxide made by the chemical reaction. Next, we seal the high-pressure tube. For experiments with initial pressures greater than 1 atm, we pressurize the high-pressure tube by connecting the tube to a high-pressure CO_2 supply. We then wait 25 min to 2 days until the bubbly corn syrup reaches to the initial vesicularity at which we desire to run the decompression experiment. At this point, we use a microscope to take a picture of the bubbles within the high-pressure tube, and near the tube wall. This time scale for the chemical reaction is much longer than the millisecond timescale for decompression, and we thus assume that the chemical reaction does not affect the expansion of the bubbly corn

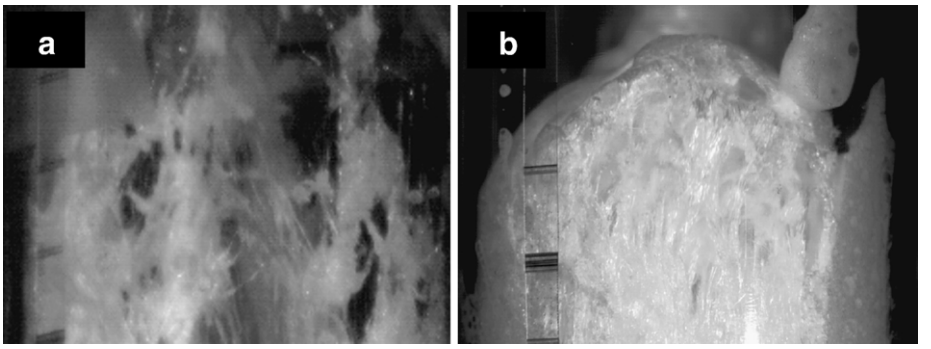

Fig. 3. Snapshots showing the deformation of the bubbly fluids during their expansion. Vertical and horizontal dimensions are 0.04 and 0.05 m, respectively. (a) Middle of the flow for a case in which the fluid fragments (t=0.047 s; ϕ_i=0.55, P_h=10^5 Pa and η_s=61 Pa s). (b) Flow front for an experiment in which the fluid does not fragment (t=0.042s; ϕ_i=0.81, P_h=10^5 Pa and η_s=2.9×10^3 Pa s). The bubbles are elongated in the vertical direction and are interconnected.

syrup during the decompression. Vesicularity is calculated from the mass and density of the corn syrup added to the high-pressure tube and the observed height of the bubbly corn syrup within the tube. When we pour the corn syrup into the high-pressure tube, a small fraction of the syrup (<10%) can adhere to upper parts of the tube wall leading to an under-estimate of the initial vesicularity. We then decrease the pressure in the low-pressure tank and the pressure difference between the low-pressure tank and high-pressure tube breaks the diaphragms. Following the rupture of the diaphragms, the bubbly fluid inside the high-pressure tube is decompressed and we record the expansion of the bubbly corn syrup with a high speed camera that can take up to 2000 pictures/s. We vary three parameters: initial pressure in the high-pressure shock tube P_h, initial vesicularity ϕ_i, and viscosity of the corn syrup η_s. Table 1 summarizes the conditions of the experiments we performed.

3. Results

3.1. Conditions for fragmentation

The conditions under which the fluid fragments can be identified by varying ϕ_i and η_s (Fig. 3). When the fluid does not fragment, permeable gas flow is sometimes documented. The height of the surface of the fluid as a function of time is shown in Fig. 4 for these two cases: first, when the fluid fragments, and second, when it becomes permeable. In general, fragmentation is observed with lower viscosity corn syrup.

In the fragmentation case, the bubbly fluid expands rapidly and at an approximately constant velocity (Fig. 4). The bubbly fluid is stretched vertically and finally tears into several pieces — it is this breakage we use to define fragmentation in our experiments. The fragmented pieces have a ragged shape (Fig. 3(a)).

If the fluid does not fragment, the fluid column expands more slowly than the fragmentation case, expansion ends at around 0.05 s, and the bubbly fluid deflates (Fig. 4). Images of the expanding fluid show vertically-elongated and interconnected bubbles (Fig. 3 (b)). These observations suggest that gas is able to escape from the bubbly fluid during the decompression.

To confirm whether outgassing occurs when the fluid does not fragment, we plot in Fig. 5 the ratio of the observed final height of the bubbly fluid to the theoretical prediction for the case in which fragmentation does not occur. The theoretical final height L_{TF}, is calculated by

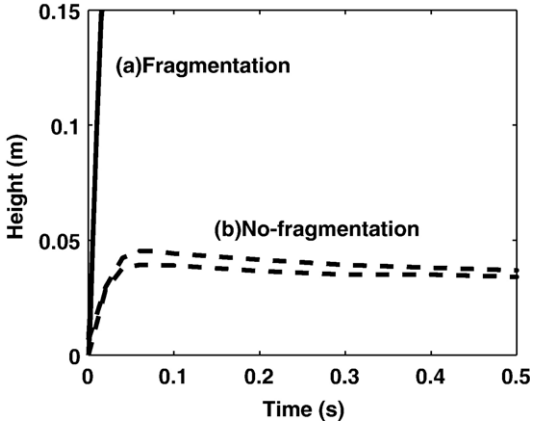

Fig. 4. Height of the top of the bubbly fluid (flow front) as a function of time. Solid and dashed curves correspond to the experiments shown in Fig. 3(a) and (b), respectively. Sometimes the upper surface of the fluid is rough, such as case b. The upper and lower dashed lines indicate the height of the flow front based on the highest and lowest points along the rough surface.

assuming that gas inside bubbles expands under isothermal condition without outgassing (Namiki and Manga, 2006)

$$L_{\mathrm{TF}} = L_{\mathrm{i}}\left\{\phi_{\mathrm{i}}\left(\frac{P_{\mathrm{h}} - P_{\mathrm{l}}}{P_{\mathrm{l}}}\right) + 1\right\}, \quad (1)$$

where L_{i} is the initial height of the bubbly fluid. The observed final height is measured at the very top of the bubbly fluid. Because the top of the fluid is sometimes curved (for example, Fig. 3(b)) the height ratio will be a maximum and it can occasionally exceed unity. Fig. 5 shows that the ratio is less than 1 in most cases even if it is a maximum estimate, suggesting that outgassing has occurred.

3.2. Expansion velocity

From the time derivative of the flow front height (Fig. 4), we obtain the expansion velocity of the bubbly fluid. Fig. 6 summarizes the measured expansion velocities. The symbol size is proportional to the product of initial vesicularity and initial pressure in the high-pressure tube $\phi_{\mathrm{i}}P_{\mathrm{h}}$, a measure of the initial potential energy available to drive expansion. The symbol type indicates whether or not the fluid fragmented. To calculate a velocity, we use three consecutive measurements of the height of the flow front. Again, we define the flow front as the maximum height of the fluid. To estimate the uncertainty on this velocity we also calculate the velocity at the same point during the expansion using 5 consecutive height measurements. Measurements are made at 0.5 to 2 ms intervals depending on the expansion velocity. The error bars on the velocity measurements we plot in Fig. 6 span the range between velocities calculated using these 3 and 5 consecutive height measurements.

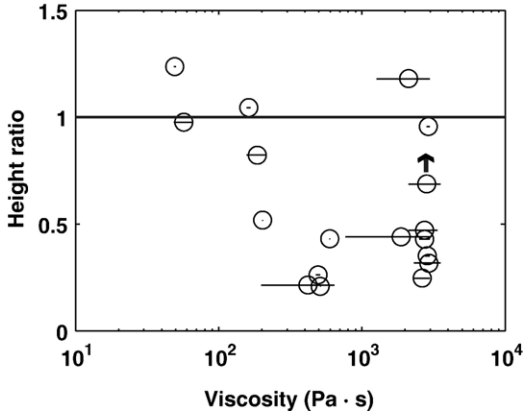

Fig. 5. Final height of the bubbly fluid divided by the theoretical estimate of the maximum possible height, Eq. (1), for experiments in which the fluid does not fragment. The theoretical estimate assumes isothermal expansion and no outgassing. Experiments whose height ratio is less than 1, indicate that outgassing has removed gas from the bubbly fluid. In the experiment denoted by an arrow, visual observations end during the expansion of the bubbly fluid. The actual final height should be larger than that denoted by the circle. The horizontal bar indicates the range of the viscosity between the measured temperature within the high-pressure tube and room temperature.

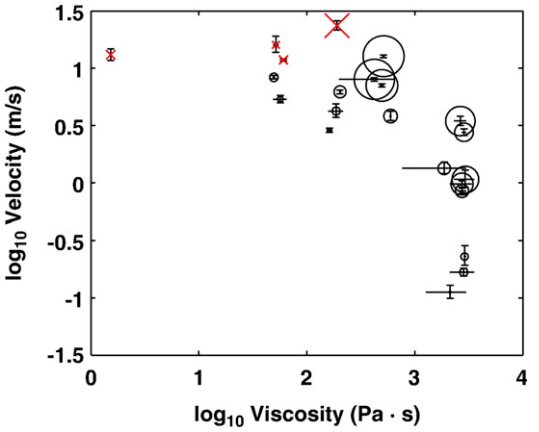

Fig. 6. Measured flow front velocity as a function of shear viscosity. Red crosses and black circles indicate experiments with and without fragmentation, respectively. The area of the symbol represents the product of initial vesicularity and initial pressure of high-pressure tube, $\phi_{\mathrm{i}}P_{\mathrm{h}}$. The error bars on the velocity indicate the calculated velocity using either three or five consecutive snapshots taken at 0.5 to 2 ms intervals. The horizontal error bars indicate the range of the viscosity between the measured temperature within the high-pressure tube and room temperature. (For interpretation of the references to colour in this figure legend, the reader is referred to the web version of this article.)

Fig. 6 shows that as the viscosity of the fluid increases, the expansion velocity decreases for a given $\phi_{\mathrm{i}}P_{\mathrm{h}}$. Large ϕ_{i} and P_{h} result in faster expansion for a given viscosity. We also find that fragmentation is associated with larger velocity for a given viscosity.

4. Discussion

Fig. 6 suggests that if the expansion velocity is large enough the bubbly fluid fragments. If the fluid does not fragment, we sometimes observe outgassing, documented by a decrease in the height of the bubbly fluid. Here, we first derive a scaling law for the expansion velocity of the bubbly fluid, then identify the criterion for fragmentation. Second, we estimate the permeability for the case in which the fluid does not fragment.

4.1. A scaling law for the expansion velocity

Fig. 6 shows that the expansion velocity depends on the viscosity, vesicularity ϕ_{i}, and initial pressure in the

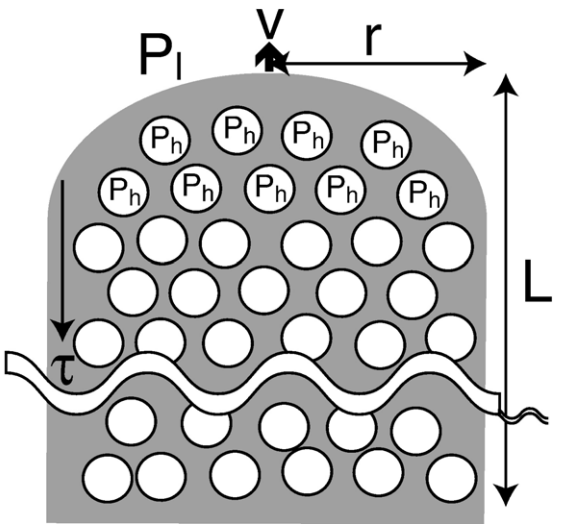

Fig. 7. Schematic illustration showing the elongation of the bubbles and forces that act on the bubbly fluid.

high pressure tube P_h. Visual observation shows that the vertically-elongated fluid column shrinks radially and detaches from the tube wall. We thus consider the elongation of a fluid column with a cylindrical shape. The expansion velocity is determined by a force balance between viscous drag to elongate the fluid column and the pressure difference driving the expansion of bubbles. Fig. 7 illustrates the geometry of this situation.

The net pressure force acting to expand the bubbly fluid vertically is given by the product of the pressure difference between the inside and outside a bubble, $(P_h - P_l)$, and the cross-sectional area of the bubbles. Here we assume that all bubbles have same radius and are distributed homogeneously, so that the radius ratio of the bubble and the outer edge of the surrounding fluid film becomes $\phi_i^{1/3}$. The cross-sectional area that consists of bubbles is thus $\pi r^2 \phi_i^{2/3}$, where r is the radius of the fluid column. Here we consider the very beginning of the expansion when the pressure will be the initial pressure of the high-pressure tube and the vesicularity is the same as the initial one. The force acting to elongate the bubbly fluid is thus $\pi r^2 \phi_i^{2/3}(P_h - P_l)$.

Viscous forces will hinder the expansion of the bubbly fluid. Because of the geometry of the expansion, rather than use the viscous resistance for a Poiseuille (pipe) flow, we evaluate the resistance to the elongation of a fluid column. The viscous force is the product of the viscous stress, $\tau = \eta_e v/L$, and the cross-sectional area of the vertically-connected fluid $\pi r^2(1-\phi_i^{2/3})$, where η_e is the elongation viscosity which is three times the shear viscosity, $\eta_e = 3\eta_s$ (Webb and Dingwell, 1990), v is the flow front velocity, L is the vertical length scale of the bubbly fluid, and the shear rate is v/L. The viscous force is thus $\pi r^2(1-\phi_i^{2/3})\eta_e v/L$.

If the expansion velocity is governed by the balance of these two forces, the velocity is

$$v = C\frac{L(P_h - P_l)}{3\eta_s\left(1/\phi_i^{2/3} - 1\right)}, \tag{2}$$

where C is a fitting parameter and we use $C = 1/2$. Fig. 8(a) shows an excellent correlation between the measured and calculated expansion velocity, indicating that Eq. (2) explains the measurements well when the flow front velocity is less than 10 m s^{-1}.

When viscous stresses no longer limit the expansion velocity, we assume that the conversion of the enthalpy change accompanying decompression to kinetic energy

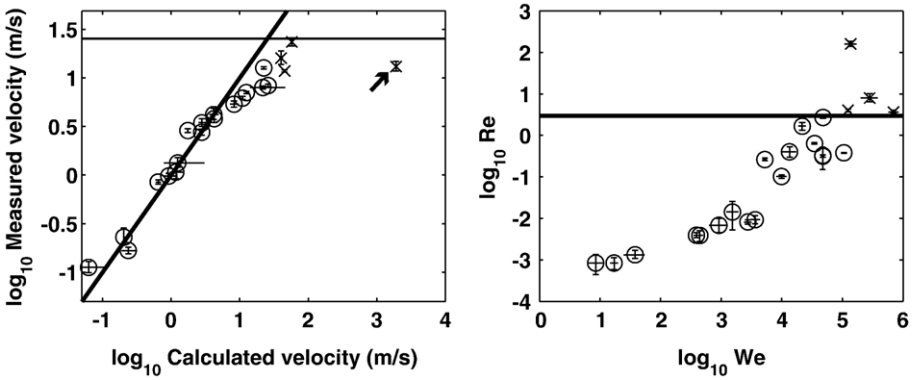

Fig. 8. (a) Measured and calculated velocities from Eq. (2). Crosses and circles indicate experiments with and without fragmentation, respectively. Thick line shows the correlation between the measured and calculated flow front velocities, given by Eq. (2). Thin line shows the maximum velocity predicted by Eq. (3) for the case indicated by the arrow. The range of the measured velocity is the same as that used in Fig. 6. The range of the calculated velocity is based on that of viscosity and the error bars are dominated by the uncertainty in viscosity. (b) Reynolds number as a function of Weber number calculated from Eqs. (4) and (5), respectively. To calculate the Reynolds and Weber numbers we use the measured flow front velocity.

governs the expansion velocity (Namiki and Manga, 2005, 2006). Converting enthalpy change to kinetic energy, we approximately obtain

$$\frac{1}{2}\rho(1-\phi_i)v^2 = \frac{\gamma\phi_i P_h}{\gamma-1}, \quad (3)$$

where ρ is the liquid density and γ is isentropic exponent assumed to be 1.3. The thin line in Fig. 8(a) shows the velocity predicted by Eq. (3) for the case denoted by the arrow. This should be the maximum possible velocity.

We thus conclude that when the viscosity is large enough, the flow front velocity is determined by Eq. (2), and when viscosity is small enough to not influence expansion, the maximum flow front velocity is given by Eq. (3).

4.2. Threshold for the fragmentation

Because the bubbly fluid continues to expand after fragmentation, we assume that the threshold is governed by the ability of viscous forces to limit expansion. This criterion can be characterized by a Reynolds number. Using Eq. (2), the Reynolds number is

$$\mathrm{Re} = \frac{\rho(1-\phi_i)vL}{\eta_e} = \frac{\rho(1-\phi_i)(P_h-P_l)L^2}{18\eta_s^2\left(1/\phi_i^{2/3}-1\right)}. \quad (4)$$

Fragmentation of low viscosity liquids also requires that surface tension forces are not too large (e.g., Villermaux, 2007). The ratio of inertial and surface tension stresses is characterized by the Weber number

$$\mathrm{We} = \frac{\rho(1-\phi_i)v^2L}{\sigma}, \quad (5)$$

where σ is surface tension and has a value of 0.07 N m^{-1} (Manga and Stone, 1995), a value similar to that of silicate melts (Khitarov et al., 1979; Mangan and Sisson, 2005). Fig. 8(b) shows that Re ~ 3 separates experiments in which fragmentation occurs. In all cases We ≫ 1 and surface tension forces can be neglected, both in our experiments and in real magmas. That is, inertial forces are sufficiently large compared to surface tension that viscous forces determine whether the fluid fragments: if Re > O(1) the bubbly fluid and magma fragments.

4.3. Permeability

If the fluid does not fragment, we can determine whether the bubbly fluid becomes permeable, and if it does, estimate the permeability. The details of the permeability calculation are described in Appendix A.1.

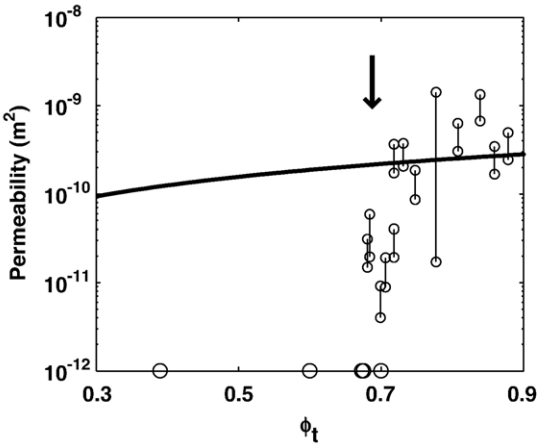

Fig. 9. Calculated permeability as a function of the time-dependent vesicularity for experiments in which the fluid does not fragment. In some cases, the permeability cannot be calculated so the maximum vesicularity, after the expansion, is shown. The thick curve shows the permeability for parallel tubes given by $\delta^2\phi_t/32$, where δ is the bubble diameter and assumed to be 10^{-4} m.

Fig. 9 shows the calculated permeability as a function of the time-dependent vesicularity ϕ_t. In some cases, the permeability cannot be determined so the maximum vesicularity is plotted. The bold curve shows the permeability predicted by a capillary tube model, $\delta^2\phi_t/32$ (e.g., Bear, 1972), where δ is the bubble diameter. Because the fluid is confined in the tube and the bubbles elongate in the vertical direction we use the bubble size prior to decompression $\delta \sim 10^{-4}$ m in the capillary tube model.

Fig. 9 shows that when the vesicularity becomes larger than 0.7, the permeability is close to that of the capillary tube model implying that the bubbles have become well-connected. Below a vesicularity around 0.7, the permeability is much smaller implying that there is a critical vesicularity for the fluid to become permeable, around 0.7. This value is similar to the close-packing volume fraction of spherical bubbles (e.g., Weaire and Hutzler, 1999). When the bubbles contact each other under the close-packed condition, the films of fluid surrounding bubbles become thin enough that bubbles can coalesce. This condition has been proposed as a fragmentation criterion (Verhoogen, 1951; Sparks, 1978; Gardner et al., 1996).

The initial vesicularity for the case shown in Fig. 3(b) is 0.81, which is larger than the proposed 0.7 threshold. The fact that such high porosity foams can be made implies that impermeable foams with vesicularity larger than 0.7 can exist. The threshold vesicularity required to develop permeability must depend on the bubble expansion time

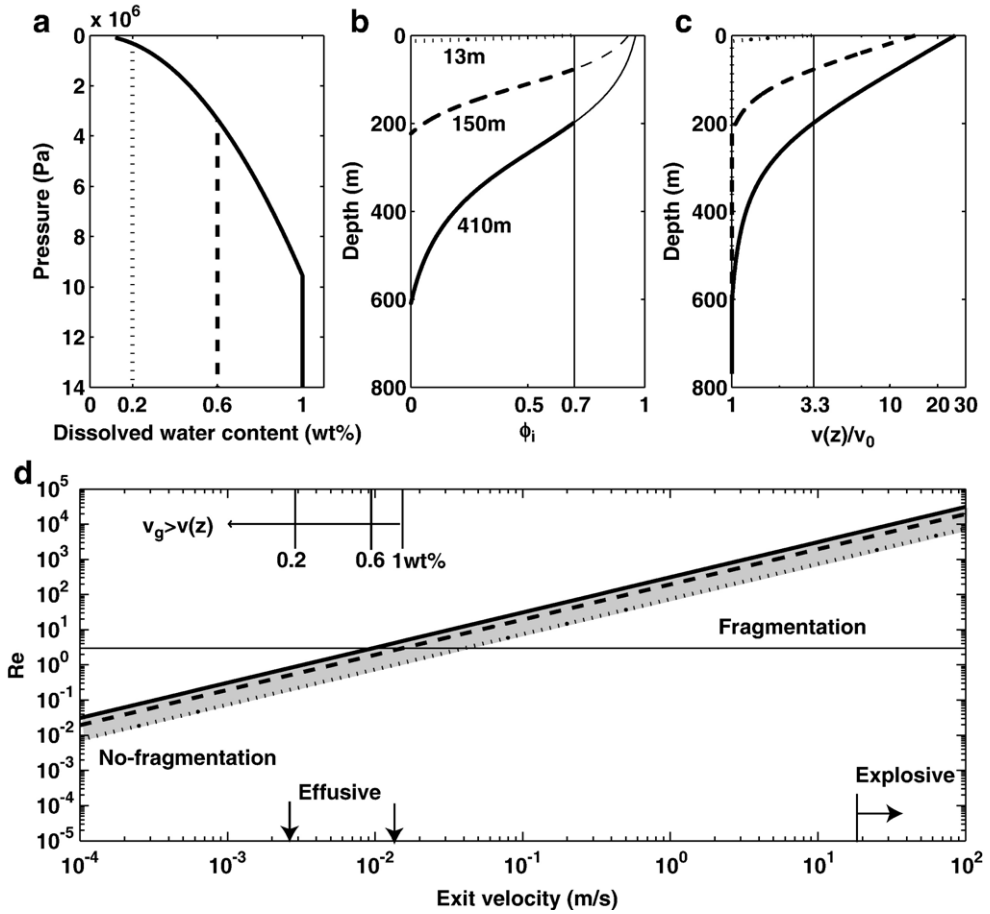

Fig. 10. (a) Dissolved water content in basaltic melt (Dixon et al., 1995) as a function of pressure. Solid, dashed and dotted curves indicate initial water fractions in the melt of 0.2, 0.6, and 1 wt.%, respectively. (b) Vesicularity as a function of depth when there is no outgassing. The bold parts of these curves show depths where the vesicularity is $0<\phi<0.7$. (c) Vertical velocity as a function of depth. (d) Solid, dashed and dotted thick lines show calculated Reynolds number as a function of the exit velocity for initial water fractions in the melt of 0.2, 0.6, and 1 wt.%, respectively. Viscosity is assumed to be 10^2 Pa s. Horizontal line shows Re=3, the experimentally determined fragmentation threshold. Vertical thin lines show the upper bound on exit velocity at which the outgassing is effective for indicated initial water content. The arrows indicate observations of exit velocities for explosive and effusive eruptions.

scale which in turn is governed by the decompression rate. For sufficiently slow expansion, the liquid surrounding bubbles can flow so that a foam with a vesicularity greater than 0.7 can be made.

The threshold of 0.7 also depends on the type of deformation experienced by the fluid. Here the flow is driven by bubble expansion in a laterally confined region. In an unconfined "parcel" of fluid, this threshold is presumably much higher, as demonstrated by the high vesicularity of reticulite (Mangan and Cashman, 1996). In simple shear flows, in contrast, bubbles can coalesce at much smaller vesicularities (Okumura et al., 2006) and magma can become permeable at vesicularities much smaller than the threshold found in our experiments.

5. Implications for basaltic eruptions

Our analogue experiments allow us to identify a fragmentation threshold for bubbly fluids with viscosities and surface tensions similar to those of basaltic magmas. We also determine the critical vesicularity at which bubble expansion causes the bubbly fluid to become permeable. As noted in Section 4.3, the nature of the flow will influence the critical vesicularity. Because the expansion of bubbles in a conduit is similar to the flow in the lab experiments, we assume that the vesicularity threshold is also appropriate for basaltic magma rising through a conduit (but not for lava flows).

Here we consider the implications of these thresholds for steady eruptions. Do the two thresholds govern the transition between explosive, e.g., fire fountaining, and effusive eruptions?

First we determine the conditions under which Re exceeds ~1. As in the lab experiments, the expansion velocity in Re is caused by decompression which increases vesicularity. Unlike the lab experiments in which preexisting gas in the bubbles expands in response to the pressure change, in basaltic magmas, bubble growth will also occur by exsolution of dissolved volatiles (assumed here to be only water). We assume an initial water content of 0.2–1 wt.%, (e.g., Johnson et al., 1994; Wallace and Anderson, 1998) and the pressure-dependent water solubility in Dixon et al. (1995). We assume that the expansion is driven by exsolution of water only, and neglect the exsolution of other gases such as CO_2.

Fig. 10(a) shows the dissolved water content as a function of pressure for initial water contents of 0.2, 0.6, and 1 wt.%. If gas bubbles do not separate from the melt, the vesicularity is given by

$$\phi = \frac{1}{\left(\frac{1}{C_e} - 1\right)\frac{\rho_w}{\rho_m} + 1}, \tag{6}$$

where C_e is the weight fraction of exsolved water and the gas density is $\rho_w = 1 \cdot (P/P_a)$ kg m^{-3}, where P is pressure and $P_a = 10^5$ Pa is atmosphere pressure. Fig. 10(b) shows vesicularity as a function of depth. To convert pressure to depth z we integrate $dP/dz = \rho_m(1-\phi)g$ with respect to z, where the density of magma $\rho_m = 2800$ kg m^{-3} (Spera, 2000), and $g = 10$ m s^{-2} is gravitational acceleration. If the radius of the conduit does not vary over the depth interval in which vesiculation and bubble growth occurs, the vertical velocity can be calculated from mass conservation

$$v(z) = \frac{v_o}{1 - \phi(z)}, \tag{7}$$

where $v(z)$ is the velocity at a depth z and v_o is the velocity at the bubble-free depth. Fig. 10(c) shows the depth-variation of velocity.

For the magma to fragment, we will assume Re must reach the threshold of ~1 before ϕ reaches the threshold of ~0.7 for the magma to become permeable. If the gas in the bubbles can escape by permeable flow, bubbles will no longer expand and fragmentation caused by expansion cannot occur. The bold curves in Fig. 10(b) show the depth range in which fragmentation driven by expansion is possible. In order to calculate a Reynolds number using Eq. (4), we need the length scale over which the fluid expands, and the velocity difference between the top and bottom of bubbly magma. For water contents of 0.2, 0.6 and 1.0 wt.%, Fig. 10(b) shows that the length scales are 13, 150, and 410 m, respectively. The velocity at the depth where vesicularity becomes 0.7 is 3.3 times that of the bubble-free region. The eruption velocity at the surface is 3.2, 14, and 26 times that of the bubble-free region for water contents of 0.2, 0.6, and 1 wt.%, respectively. We thus can estimate the velocity difference in Eq. (4) as a function of the exit velocity at the surface. Viscosity of basaltic magma depends on temperature and water content (e.g., Spera, 2000; Giordano and Dingwell, 2003); we assume $\eta = 10^2$ Pa s, which is appropriate for dry basalt at 1200 °C.

Fig. 10(d) shows the Reynolds number as a function of the exit velocity. This figure shows that exit velocities around 10^{-2} m s^{-1} correspond to the threshold for fragmentation. The exit velocity v_e for explosive eruption can be estimated from the fountain height h by $v_e = \sqrt{2gh}$. Observed fountain heights range from few tens to several hundred meters (e.g., Swanson et al., 1979; Wolfe et al., 1989) and the corresponding eruption velocity exceeds 15 m s^{-1}. For the velocity of effusive eruptions, we use Vergniolle and Jaupart's compilation (Vergniolle and Jaupart, 1986): 2.5×10^{-3} m s^{-1} for Etna and 1.2×10^{-2} m s^{-1} for Mauna Ulu. For a plausible range of initial water contents, the calculated threshold governed by a critical Reynolds number is consistent with the natural observations.

Next, we determine whether outgassing is effective at removing gases driving the eruption when ϕ exceeds the permeability threshold $\phi \sim 0.7$. We can compare the rate at which pressure in the gas is changing with the rate at which the gases can escape from the magma. For the exsolution

$$\frac{dP}{dt} = \frac{dP}{dz} \cdot \frac{dz}{dt} = \rho_m g(1-\phi) \cdot v(z). \tag{8}$$

For the permeable gas flow (e.g., Ingebritsen and Sanford, 1998),

$$\phi\beta\frac{\partial P}{\partial t} = \frac{k}{\eta_g}\frac{\partial^2 P}{\partial z^2}, \tag{9}$$

where k is permeability, η_g is gas viscosity, β is compressibility of gas, and we neglect compressibility of the bulk magma. From Eqs. (8) and (9), when

$$v(z) \ll \frac{k}{\eta_g \phi\beta\rho_m g(1-\phi)}\frac{d^2P}{dz^2}, \tag{10}$$

outgassing should be very efficient. We can determine this condition by using a permeability of 10^{-11} m^2 based

on our experiments and measurements on basaltic rocks (e.g., Saar and Manga, 1999), $\eta_g = 5 \times 10^{-5}$ Pa s for gas at 1000 °C, a critical vesicularity to have permeability of $\phi = 0.7$, and $d^2P/dz^2 = -\rho_m g \, d\phi/dz$. The calculated ascent velocity at the depth where $\phi = 0.7$ can be converted to exit velocity using Fig. 10(c). The maximum exit velocity at which the outgassing becomes effective is shown in Fig. 10(d). The predicted limits for water contents in the range of 0.2 to 1.0 wt.% fall close to the threshold for fragmentation ($Re \sim 1$), suggesting that when the magma fails to fragment, the gas trapped in magma can readily escape by outgassing.

We conclude that the bifurcation of the eruption style can be explained by the combination of two thresholds. When Re exceeds the threshold for inertia-driven fragmentation the eruption style becomes explosive. On the other hand when Re does not exceed the threshold, effective outgassing occurs and the eruption style is effusive. Our experimentally determined fragmentation threshold appears to be consistent with conditions that separate effusive and explosive basaltic eruptions.

6. Concluding remarks

In our experiments we can identify two thresholds that should govern the transition between explosive and effusive eruption of basaltic magmas. The fragmentation threshold is given by a critical Reynolds number that characterizes the importance of inertial forces generated by the expansion of bubbles. We also find a vesicularity threshold above which bubble expansion causes the bubbly fluid to become permeable. The ascent velocity governs the Reynolds number, implying that the explosibility depends on the ascent rate of the magma (Wilson and Head, 1981; Parfitt et al., 1995; Namiki and Manga, 2006).

In the traditional view of fragmentation, high viscosity promotes fragmentation, either because it hinders bubble growth which leads to large tensile stress within the melt surrounding bubbles (Zhang, 1999; Koyaguchi and Mitani, 2005), or because the deformation rate exceeds the inverse relaxation time of the melt (Webb and Dingwell, 1990; Papale, 1999). Our experimental results show that decreasing viscosity can promote fragmentation by allowing inertia to become dynamically important. This result is consistent with the observation that lower viscosity magma is associated with higher explosion intensity for basaltic magma (Lautze and Houghton, 2007). Using Eq. (4), we can estimate the viscosity range in which inertia-driven fragmentation can occur. Assuming general conditions for magma, $\rho = 2800$ kg m^{-3}, $\phi_i = 0.6$, $P_h = 10^6$ Pa, and $L = 400$ m from Fig. 10, when the viscosity is less than 10^6 Pa s, inertia-driven fragmentation can occur. We thus summarize the fragmentation regime in Fig. 11. When the viscosity of magma is $> 10^6$ Pa s, brittle fragmentation can occur. On the other hand, when the viscosity of magma is less than 10^6 Pa s, inertia-driven fragmentation can occur. In this latter case, the magma is stretched and tears. As a result, the shape of the magma fragments will differ from that made by brittle fragmentation (Heiken and Wohletz, 1985; Taddeucci et al., 2007). Pele's hair and tears are presumably examples of fragments formed in this manner. Unfortunately, our current experimental design does not allow us to characterize clast shape and size distribution but we might expect clast attributes to be different for brittle and inertia-driven fragmentation. Characterizing the shape of these fragments may provide a means to use field deposits to identify fragmentation mechanisms.

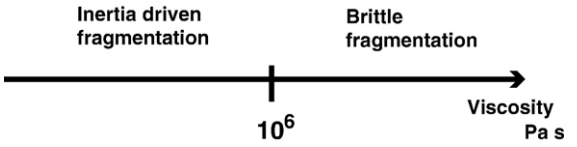

Fig. 11. Schematic illustration of the fragmentation style as a function of viscosity. In the brittle fragmentation regime, magma fails as a solid material. In the inertia-driven regime, magma is stretched and tears.

Acknowledgements

We thank S. Mueller and anonymous reviewer for comments and H. M. Gonnermann for critical reading of an earlier version of this manuscript. A. N. has been supported by JSPS. This work is supported by NSF EAR 0439765.

Appendix A.1. Estimate of the permeability

We use the time-evolution of the height of the bubbly fluid (Fig. A.1(a)) along with measured pressures to calculate bounds on the permeability. We assume that the pressure at the top of the bubbly fluid falls immediately to the pressure of the low-pressure tank P_l and maintains a constant value following the rupture of the diaphragms. The pressure P_h at the bottom of the fluid column is measured (Fig. A.1(b)).

We estimate the pressure distribution in the bubbly fluid two ways: (1) a linear decrease from P_h to P_l, and (2) constant value of P_h. These will lead to minimum and maximum bounds on the calculated permeability, respectively, and we refer to these limits as "linear" and "maximum" estimates. We also assume that temperature

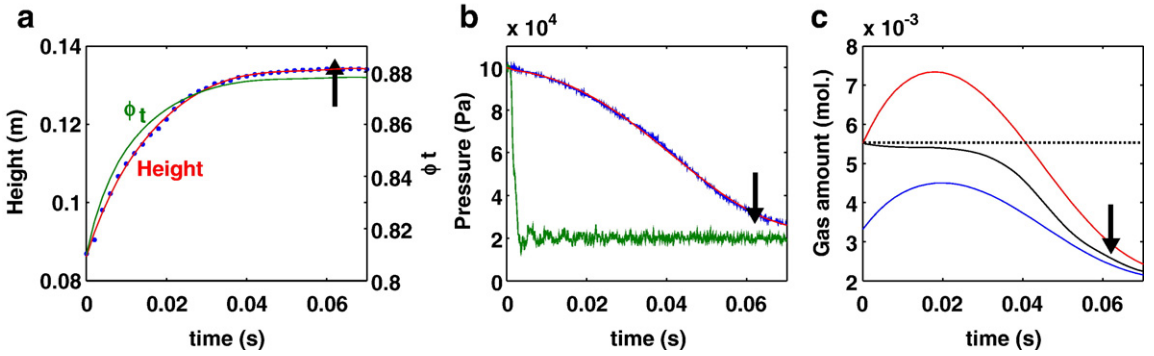

Fig. A.1. Measured and estimated properties for the case shown in Fig. 3(b). (a) Blue dots show the measured height of the bubbly fluid. Red curve is a curve fitted to the data. Green curve is the calculated time-dependent vesicularity given by Eq. (13). (b) Blue and green curves show the measured pressure change after the diaphragm breaks at the top and the bottom of the bubbly fluid, respectively. Red curve is fitted to the measured bottom pressure. (c) Blue and red curves show the estimated minimum and maximum amount of gas stored in the bubbly fluid predicted by Eqs. (11) and (12), respectively. (For interpretation of the references to colour in this figure legend, the reader is referred to the web version of this article.)

in the bubbly fluid remains constant at T_0, which is measured by a thermocouple.

The amounts of gas trapped in the foam for linear and maximum estimates are given by

$$n_{Lt} = \phi_t \frac{\pi r^2}{RT_0} \frac{P_\mathrm{l} + P_\mathrm{ht}}{2} L_t \tag{11}$$

$$n_{Mt} = \phi_t \frac{\pi r^2}{RT_0} P_\mathrm{ht} L_t, \tag{12}$$

where n is amount of gas in moles, r is the radius of the high-pressure tube, R is the gas constant, and L is the height of the bubbly fluid. Subscripts L, M, and t denote the linear model, maximum model, and time-dependent value, respectively. The time-dependent vesicularity ϕ_t is calculated by assuming that the liquid volume is constant,

$$L_t(1-\phi_t) = L_\mathrm{i}(1-\phi_\mathrm{i}). \tag{13}$$

The green curve in Fig. A.1(a) shows the calculated vesicularity.

The volume flux of gas discharged from the top of the bubbly fluid at time t for each estimate is given by the time derivative of the gas amount in the bubbly fluid $q_t = -(RT_0/P_\mathrm{l})\mathrm{d}n_t/\mathrm{d}t$. The velocity of gas discharged from the bubbly fluid for these two models is

$$v_{Lt} = -\frac{1}{2P_\mathrm{l}}\{L_t - L_\mathrm{i}(1-\phi_\mathrm{i})\}\frac{dP_\mathrm{ht}}{dt} - \frac{P_\mathrm{l} + P_\mathrm{ht}}{2P_\mathrm{l}}\frac{dL_t}{dt} \tag{14}$$

$$v_{Mt} = -\frac{1}{P_\mathrm{l}}\{L_t - L_\mathrm{i}(1-\phi_\mathrm{i})\}\frac{dP_\mathrm{ht}}{dt} - \frac{P_\mathrm{ht}}{P_\mathrm{l}}\frac{dL_t}{dt}. \tag{15}$$

Fig. A.1(c) shows the estimated amount of gas trapped in the bubbly fluid. The red curve shows that the maximum estimate exceeds the initial value and is clearly unrealistic. This results from our assumption of constant pressure within the fluid column, whereas the top part of the fluid column should be at lower pressure than at the bottom. The base of the tube is an impermeable plate with no gas flux, requiring that the pressure gradient at the bottom of the bubbly fluid is zero. For this reason the linear model shown in blue provides the lower bound on the amount of gas in the bubbly fluid. We thus assume that the total amount of gas in the bubbly fluid lies somewhere between the red and blue curves, and likely resembles the (hand drawn) black curve. Because the red curve falls below the initial value at $t=0.04$ s, some gas must be discharged from the bubbly fluid indicating that it is permeable. If the pressure profile within the bubbly fluid does not change significantly, the time derivative of the red and blue curves provide the maximum and minimum estimates of the discharge rates. We thus regard v_{Mt} and v_{Lt} as the maximum and minimum discharge velocities, respectively.

Next we calculate the permeability from v_{Mt} and v_{Lt}. Darcy's equation, modified to account for compressibility of the gas and inertia of the gas, is

$$\frac{\eta_\mathrm{g}}{k_1} v_t + \frac{\rho_\mathrm{o}}{k_2} v_t^2 - \frac{P_\mathrm{ht}^2 - P_\mathrm{l}^2}{2P_\mathrm{l}L_t} = 0, \tag{16}$$

where k_1 is the Darcian permeability, k_2 is the inertial permeability which has a dimension of length scale, ρ_o is the density of gas at the top of the bubbly fluid, and η_g is the gas viscosity. We assume $\rho_\mathrm{o} = 1$ kg m^{-3} at 10^5 Pa, isothermal expansion of the gas, $\eta_\mathrm{g} = 10^{-5}$ Pa s, and we neglect the pressure dependence of viscosity.

Rust and Cashman (2004) measured k_1 and k_2 for obsidian flow and pumice samples, and found a relation between k_1 and k_2,

$$k_2 = 4.75 \times 10^{14} k_1^{1.87}. \quad (17)$$

Muller et al. (2005) measured the permeability of dome samples and obtained results consistent with those of Rust and Cashman (2004). We thus combine Eqs. (16) and (17) and solve the resulting equation numerically to obtain the permeability k_1.

Fig. 9 shows k_1 calculated from v_{Mt} and v_{Lt} as maximum and minimum estimates, respectively. We calculate k_1 when the bottom pressure falls to 90% of $P_h - P_l$, as indicated by the arrows in Fig. A.1.

References

Barclay, J., Riley, D.S., Sparks, R.S.J., 1995. Analytical models for bubble growth during decompression of high viscosity magmas. Bull. Volcanol. 57, 422–431.

Bear, J., 1972. Dynamics of Fluids in Porous Media. Dover Publications, Inc., New York. 764 pp.

Dixon, J.E., Stolper, E.M., Holloway, J.R., 1995. An experimental study of water and carbon dioxide solubilities in mid-ocean ridge basaltic liquids. Part I: calibration and solubility models. J. Petrol. 36, 1607–1631.

Eichelberger, J.C., Carrigan, C.R., Westrich, H.R., Price, R.H., 1986. Non-explosive silicic volcanism. Nature 323, 598–602.

Gardner, J.E., Thomas, R.M.E., Jaupart, C., Tait, S., 1996. Fragmentation of magma during Plinian volcanic eruptions. Bull. Volcanol. 58, 144–162.

Gardner, J.E., Hilton, M., Carroll, M.R., 2000. Bubble growth in highly viscous silicate melts during continuous decompression from high pressure. Geochim. Cosmochim. Acta 64, 1473–1483.

Giordano, D., Dingwell, D.B., 2003. Viscosity of hydrous Etna basalt: implications for Plinian-style basaltic eruptions. Bull. Volcanol. 65, 8–14.

Gonnermann, H.M., Manga, M., 2003. Explosive volcanism may not be an inevitable consequence of magma fragmentation. Nature 426, 432–435.

Goto, A., 1999. A new model for volcanic earthquake at Unzen volcano: melt rupture model. Geophys. Res. Lett. 26, 2541–2544.

Heiken, G., Wohletz, K., 1985. Volcanic ash. University of California Press, Berkeley. 246 pp.

Houghton, B.F., Wilson, C.J.N., Carlo, P.D., Coltelli, M., Sable, J.E., Carey, R., 2004. The influence of conduit processes on changes in style of basaltic Plinian eruptions: Tarawera 1886 and Etna 122 BC. J. Volcanol. Geotherm. Res. 137, 1–14.

Ingebritsen, S.E., Sanford, W.E., 1998. Groundwater in Geologic Processes. Cambridge University Press, Cambridge, UK. 341 pp.

Johnson, M.C., Anderson, A.T., Rutherford, M.J., 1994. Pre-eruptive volatile contents of magma. Rev. Miner. 30, 281–330.

Khitarov, N.I., Lebedev, Y.B., Dorfman, A.M., Bagdasarov, N.S., 1979. Effects of temperature, pressure, and volatiles on the surface tension of molten basalt. Geochem. Int. 16, 78–86.

Klug, C., Cashman, K.V., 1996. Permeability development in vesiculating magmas: implications for fragmentation. Bull. Volcanol. 58, 87–100.

Koyaguchi, T., Mitani, N.K., 2005. A theoretical model for fragmentation of viscous bubbly magmas in shock tubes. J. Geophys. Res. 110, B10202. doi:10.1029/2004JB003513.

Lautze, N.C., Houghton, B.F., 2007. Linking variable explosion style and magma textures during 2002 at Stromboli volcano, Italy. Bull. Volcanol. 69, 445–460.

Lensky, N.G., Navon, O., Lyakhovsky, V., 2004. Bubble growth during decompression of magma: experimental and theoretical investigation. J. Volcanol. Geotherm. Res. 129, 7–22.

Mader, H.M., Brodsky, E.E., Howard, D., Sturtevant, B., 1997. Laboratory simulations of sustained volcanic eruptions. Nature 388, 462–464.

Manga, M., Stone, H.A., 1995. Low Reynolds number motion of bubbles, drops and rigid spheres through fluid-fluid interfaces. J. Fluid Mech. 287, 279–298.

Mangan, M.T., Cashman, K.V., 1996. The structure of basaltic scoria and reticulite and inferences for vesiculation, foam formation, and fragmentation in lava fountains. J. Volcanol. Geotherm. Res. 73, 1–18.

Mangan, M., Sisson, T., 2005. Evolution of melt–vapor surface tension in silicic volcanic systems: experiments with hydrous melts. J. Geophys. Res. 110, B01202. doi:10.1029/2004JB003215.

McBirney, A.R., Murase, T., 1970. Factors governing the formation of pyroclastic rocks. Bull. Volcanol. 34, 372–384.

Muller, S., Melnik, O., Spieler, O., Scheu, B., Dingwell, D.B., 2005. Permeability and degassing of dome lavas undergoing rapid decompression: an experimental determination. Bull. Volcanol. 67, 526–538.

Namiki, A., Manga, M., 2005. Response of a bubble bearing viscoelastic fluid to rapid decompression: implications for explosive volcanic eruptions. Earth Planet. Sci. Lett. 236, 269–284.

Namiki, A., Manga, M., 2006. Influence of decompression rate on the expansion velocity and expansion style of bubbly fluids. J. Geophys. Res. 111, B11208. doi:10.1029/2005JB004132.

Navon, O., Chekhmir, A., Lyakhovsky, V., 1998. Bubble growth in highly viscous melts: theory, experiments, and autoexplosivity of dome lavas. Earth Planet. Sci. Lett. 160, 763–776.

Okumura, S., Nakamura, M., Tsuchiyama, A., 2006. Shear-induced bubble coalescence in rhyolitic melts with low vesicularity. Geophys. Res. Lett. 33, L20316. doi:10.1029/2006GL027347.

Papale, P., 1999. Strain-induced magma fragmentation in explosive eruptions. Nature 397, 425–428.

Parfitt, E.A., Wilson, L., Neal, C.A., 1995. Factors influencing the height of Hawaiian lava fountains: implications for the use of fountain height as an indicator of magma gas content. Bull. Volcanol. 57, 440–450.

Proussevitch, A.A., Sahagian, D.L., 1996. Dynamics of coupled diffusive and decompressive bubble growth in magmatic systems. J. Geophys. Res. 101, 17447–17455.

Roggensack, K., Hervig., R.L., McKnight, S.B., Williams, S.N., 1997. Explosive basaltic volcanism from Cerro Negro volcano: influence of volatiles on eruptive style. Science 277, 1639–1642.

Rust, A.C., Cashman, K.V., 2004. Permeability of vesicular silicic magma: inertial and hysteresis effects. Earth Planet. Sci. Lett. 228, 93–107.

Saar, M.O., Manga, M., 1999. Permeability–porosity relationship in vesicular basalts. Geophys. Res. Lett. 26, 111–114.

Saar, M.O., Manga, M., Cashman, K.V., Fremouw, S., 2001. Numerical models of the onset of yield strength in crystal–melt suspensions. Earth Planet. Sci. Lett. 187, 367–379.

Sable, J.E., Houghton, B.F., Wilson, C.J.N., Carey, R.J., 2006. Complex proximal sedimentation from Plinian plumes: the example of Tarawera 1886. Bull. Volcanol. 69, 89–103.

Sparks, R.S.J., 1978. The dynamics of bubble formation and growth in magmas: a review and analysis. J. Volcanol. Geotherm. Res. 3, 1–37.

Spera, F.J., 2000. Physical properties of magma. In: Sigurdsson, H. (Ed.), Encyclopedia of Volcanoes. Academic Press, San Diego, pp. 171–190.

Swanson, D.A., Duffield, W.A., Jackson, D.B., Peterson, D.W., 1979. Chronological narrative of the 1969–71 Mauna Ulu eruption of Kilauea volcano, Hawaii. U. S. Geol. Surv. Prof. Pap. 1056, 1–55.

Taddeucci, J., Scarlato, P., Andronico, D., Cristaldi, A., Buttner, R., Zimanowski, B., Kuppers, U., 2007. Advances in the study of volcanic ash. EOS 88, 253–260.

Takeuchi, S., Nakashima, S., Tomiya, A., Shinohara, H., 2005. Experimental constraints on the low gas permeability of vesicular magma during decompression. Geophys. Res. Lett. 32, L10312. doi:10.1029/2005GL022491.

Thomas, N., Jaupart, C., Vergniolle, S., 1994. On the vesicularity of pumice. J. Geophys. Res. 99, 15633–15644.

Toramaru, A., 1995. Numerical study of nucleation and growth of bubbles in viscous magmas. J. Geophys. Res. 100, 1913–1931.

Tuffen, H., Dingwell, D.B., Pinkerton, H., 2003. Repeated fracture and healing of silicic magma generate flow banding and earthquakes? Geology 31, 1089–1092.

Vergniolle, S., Jaupart, C., 1986. Separated two-phase flow and basaltic eruptions. J. Geophys. Res. 91, 12842–12860.

Verhoogen, J., 1951. Mechanics of ash formation. Am. J. Sci. 249, 729–739.

Villermaux, E., 2007. Fragmentation. Annu. Rev. Fluid Mech. 39, 419–446.

Wallace, P.J., Anderson, A.T., 1998. Effects of eruption and lava drainback on the H_2O contents of basaltic magmas at Kilauea volcano. Bull. Volcanol. 59, 327–344.

Weaire, D., Hutzler, S., 1999. The Physics of Foams. Oxford University Press, New York, USA. 246 pp.

Webb, S.L., Dingwell, D.B., 1990. Non-Newtonian rheology of igneous melts at high stresses and strain rates: experimental results for rhyolite, andesite, basalt, and nephelinite. J. Geophys. Res. 95, 15695–15701.

Wilson, L., Head, J.W., 1981. Ascent and eruption of Basaltic magma on the Earth and Moon. J. Geophys. Res. 86, 2971–3001.

Wolfe, E.W., Garcia, M.O., Jackson, D.B., Koyanagi, R.Y., Neal, C.A., Okamura, A.T., 1989. The Puu Oo eruption of Kilauea volcano, epiodes 1–20, January 3, 1983, to June 8, 1984. U. S. Geol. Surv. Prof. Pap. 1350, 471–508.

Zhang, Y., 1999. A criterion for the fragmentation of bubbly magma based on brittle failure theory. Nature 402, 648–650.